

See discussions, stats, and author profiles for this publication at: <https://www.researchgate.net/publication/377721828>

# Flatness-based sliding mode control for stabilizing a spherical pendulum on a quadrotor

Article in *Asian Journal of Control* · January 2024

DOI: 10.1002/asjc.3308

---

CITATIONS

2

READS

111

2 authors:



Adrian Humberto Martinez Vasquez

Center for Research and Advanced Studies of the National Polytechnic Institute

8 PUBLICATIONS 59 CITATIONS

[SEE PROFILE](#)



Rafael Castro-Linares

Center for Research and Advanced Studies of the National Polytechnic Institute

138 PUBLICATIONS 1,975 CITATIONS

[SEE PROFILE](#)

# Flatness-based sliding mode control for stabilizing a spherical pendulum on a quadrotor

Adrian Humberto Martinez-Vasquez  | Rafael Castro-Linares 

Department of Electrical Engineering,  
 Mechatronics Section, CINVESTAV,  
 Mexico City, Mexico

## Correspondence

Rafael Castro-Linares, Department of  
 Electrical Engineering, Mechatronics  
 Section, CINVESTAV, Mexico City, Mexico.  
 Email: rcastro@cinvestav.mx

## Funding information

This research was partially supported by  
 CONAHCYT Mexico under Project  
 CB-254329.

## Abstract

This paper presents the problem of transporting a suspended load by a quadrotor. A full model considering the quadrotor and the dynamics of the suspended load, in a three-dimensional space, is proposed considering as control inputs the torques and the thrust force due to the motors. The solution proposed consists of simple control strategies based on the tangent linearization of the model, which is controllable and therefore flat. A sliding mode control technique is developed for the thrust force and torques associated with the Euler angles in order to track a desired trajectory of the vehicle in a three-dimensional space with minimum oscillation of the suspended load. The control strategy results to be relatively simple to implement and achieves local stability of the tracking errors, as well as robustness to internal nonlinearities, which are neglected in the linearization process and other external disturbances. The attractiveness of the sliding surfaces and the stability of the tracking errors are formally studied using Lyapunov stability theory. Simulation results are given to show the performance of the proposed control strategy.

## KEYWORDS

differential flatness, nonlinear systems, sliding mode control

## 1 | INTRODUCTION

The unmanned aerial vehicle (UAV) issue has had a fast growing in the last decade in the field of control theory and its applications. In particular, the quadrotor has been used by researchers to explore and apply different control strategies ranging from theoretical to practical, due to its versatility in hovering, vertical take-off, and landing. Many applications involve tasks as surveillance and reconnaissance [1, 2], trajectory tracking problem [3–5], vision guidance [6–8], among others. However, an interesting application that is currently being extensively investigated

Adrian Humberto Martinez-Vasquez and Rafael Castro-Linares are equally contributing authors.

with the quadrotor is to transport loads from one place to another, where in this task it can be carried out in two different configurations. The first configuration consists in using a gripper [9–11] to hold the load to the quadrotor as close to its center of gravity and transporting it; this configuration causes the quadrotor to have little agility in flight maneuvers due to the excess weight of the system. The second configuration is to hold the load through a cable anchored closer to the geometric center and center of gravity of the quadrotor, allowing greater agility of the vehicle but generating a pendular oscillation of the load due to the flight maneuvers of the quadrotor. The problem of the quadrotor with suspended load has been studied by researchers in recent years. This problem has character-

istics that make it very attractive for the area of control theory since the mathematical model associated to it is nonlinear, underactuated, and presents multiple inputs and multiple outputs (MIMO). The problems that involve pendulums and oscillatory motions have been widely studied in the control theory area. Some examples of these research can be found in earlier studies [12–14], where different configurations are described giving rise to multiple solutions in terms of control theory. However, the control problem of such systems is still open.

Indeed, the pendulum oscillation problem is very attractive to researchers, even when some physical configuration is added to this type of problem that makes it more complicated and challenging from the perspective of mathematical modeling and control theory. This is the case of the quadrotor which is an underactuated system with six variables to be controlled and with only four control inputs. Besides, if a cable with a suspended load is attached to this system, close to the geometric and gravity center, the system becomes more challenging because two variables to be controlled are added, namely, the angular position and the angular velocity of the suspended load, keeping the same original control inputs in the quadrotor.

The quadrotor with suspended load is a MIMO nonlinear under actuated system, and it is currently the object of study by many researchers in the world. This system introduces more degrees of freedom in horizontal motion due to the effect of the suspended load, in addition to a vertical dynamics that is associated to the flight capacity of the system and that is also coupled to the horizontal motion of the quadrotor; the thrust force generated by the propellers and the motors induces aerodynamics effects in the horizontal and vertical movements of the vehicle as well as in the oscillation of the suspended load. Many strategies and control schemes have been proposed to study this problem. In Barikbin and Fakharian [15], three controls strategies are compared: backstepping, conventional sliding mode, and super twisting integral sliding mode in the presence of disturbances and uncertainties. In that research, the authors show that super twisting method works better for the reject of uncertainties and disturbances effects. In Guerrero et al. [16], an interconnection damping assignment passivity-based control (IDA-PBC), for the transportation of a suspended payload from point to point, is presented, showing simulations results for the planar case. In Guerrero et al. [17] and Guerrero-Sánchez et al. [18], the same problem is addressed using the IDA-PBC strategy for the three-dimensional case with real-time experiments. In Guerrero-Sánchez et al. [19], two novel nonlinear control schemes for the quadrotor with suspended load problem are proposed, namely, a proportional and derivative (PD) control with a nonlinear coupled term and a nonlinear coupling control based on the first algorithm, together

with simulations results. In Mosco-Luciano et al. [20], a combination of feedback linearization and the backstepping technique is proposed to solve the trajectory tracking problem for the quadrotor with suspended load, and simulation results are presented to validate the control scheme. In Liang et al. [21], an improved adaptive control scheme is proposed to reduce large overshoots and achieve effective payload swing suppression. Experimental results are provided to show the performance in the presence of disturbances. A second-order sliding mode control strategy for a quadrotor in a three-dimensional space with suspended load is proposed in Bingöl and Güzey [22], and simulations results are presented to guarantee the effective performance of the method. In Sun et al. [23], the stability of the quadrotor load system in hovering and level flights is studied so that the expected trajectory for the quadrotor load system is computed; a hierarchical terminal sliding mode control scheme is designed to ensure the convergence of the tracking error to zero in finite time and to enhance robustness in the presence of system uncertainties and external disturbances. In Sierra-García and Santos [24], an intelligent control strategy is proposed and applied to an UAV with a cable-suspended load; the main contribution is that an artificial neural network is included to estimate the external disturbance generated by the cable-suspended load. This allows the UAV to successfully follow different trajectories with small tracking error. Control strategies based on the property of differential flatness with a cable-suspended load on a quadrotor are found [25]; the approach has been extended to include cooperation between multiple quadrotors as it is presented in Kotaru et al. [26]. Also, other types of techniques, such as the active disturbance rejection control (ADRC) approach, have been developed, where the swing of the suspended load is considered to be an external disturbance [27]. In a similar way, a double ADRC control strategy that attenuates the influence of the load swing and external disturbances on a quadrotor is proposed in Wang et al. [28]. A solution to the problem in a quadrotor carrying a payload flying through a narrow window, with the assumption that its complex dynamics model derived is unavailable, is presented in Minhuhan et al. [29]. Moreover, a robust model predictive control (MPC) technique is presented in Gaetano et al. [30], for a multibody slung-load system considering a swarm of autonomous multicopters which are connected by wires to a suspended payload; the control system is composed by different control modules to solve trajectory planning, trajectory tracking, and velocity and attitude control, while taking into account multicopter performance constraints, obstacle avoidance constraints, and computational cost. A similar scheme is employed in Son et al. [31] to control a multirotor with a slung load, where a sequential linear quadratic model

predictive control (SLQ-MPC) algorithm to control a multirotor with a slung load system, with the consideration of waypoints and obstacle avoidance in a cost function; the proposed algorithm is presented via numerical simulations. In Ubbink and Engelbrecht [32], it is presented the design of a trajectory planner and feedback control system to autonomously navigate a quadrotor UAV with a suspended payload through a confined environment consisting of horizontal and vertical tunnels; the trajectory planning task is formulated as an optimal control problem. In Danial and Hamidreza [33], it is proposed an optimal trajectory for carrying the maximum payload with minimum oscillation; the ratio of cable length to quadrotor length is used for increasing the maximum payload carrying capacity and reducing the maximum oscillation angle of the suspended load. In Urbina-Brito et al. [34], it is designed a model-based predictive control (MPC) design for a quadrotor aerial vehicle with a suspended load; the controller takes into account the hanging payload dynamics, the dynamics in a three-dimensional space, and the vehicle rotation, achieving a good balance between fast stabilization times and small swing angles; the constrained MPC strategy considered the limits on the swing angles and the quadrotor position to stabilize the aerial vehicle managing to attenuate the oscillation of the load while following a reference trajectory, considering a maximum oscillation range. In Guerrero-Sánchez et al. [35], it is presented a methodology to solve the problem of robustification based on the interconnection and damping assignment passivity-based control (IDA-PBC) scheme for the case of underactuated systems with inertia matrix dependent of the unactuated coordinates. The authors apply the proposed robust IDA-PBC strategy to an UAV that transports a payload suspended by a cable aiming to stabilize the PVTOL position and attenuate the swing angle of the payload; simulations have shown that the performance of the proposed robust control strategy is satisfactory, despite of the existence of constant external disturbances. In Godbole and Subbarao [36], it is considered the load to be a disturbance; the solution is presented through the implementation of a passivity-based controller and an extended state observer based on active disturbance rejection controller. Finally, the control technique based on sliding modes is the subject of research as can be seen in Abro et al. [37], Sira Ramírez et al. [38], and Hu et al. [39].

Based on the studies mentioned above, the present article addresses the problem of transporting an oscillating suspended pendulum by means of a cable attached to a quadrotor. The dynamic model of this system presents particular characteristics induced by the motion dynamics of the suspended load which is directly coupled to the dynamic model of the quadrotor. The challenge of controlling this system lies in the fact that the control inputs corre-

spond to the same inputs used in a conventional quadrotor; this is the thrust forces due to the motors and the torques associates with the Euler angles (roll, pitch, and yaw). Therefore, by means of these control inputs, the quadrotor is first stabilized in the orientation (Euler angles) and then horizontal and vertical translational displacements are controlled together with the oscillation movement of the suspended load so that a given trajectory is followed by the quadrotor. The complexity of the problem is reduced by making two assumptions. First, from the symmetry of the system, the longitudinal dynamics is considered to evolve in the reference frame  $X - Z$  or in a similar way in the  $Y - Z$  frame (see Figure 1). Second, it is assumed that the vehicle performs smooth maneuvers by considering that the Euler angles are small. Under these assumptions, the system can be linearized around an equilibrium point (tangent linearization), greatly simplifying the complexity of the system. The control problem is then feasibly approached since the linearization of the system is found to be controllable around an arbitrary equilibrium point and then flat [40]. The flatness of this linear system is taken into account in the design of sliding mode control strategies for the orientation and horizontal translational motion of the system, allowing to drive it substantially away from the point of operation; tracking trajectory in the  $X - Z$  frame and in the  $Y - Z$  frame is achieved guaranteeing, at the same time, oscillation attenuation of the suspended load or spherical pendulum. The insensitivity to parameter variations of the sliding mode control scheme and its robustness to disturbances such as internal (endogenous) perturbations, which were neglected in the linearization process, as well as to external (exogenous) disturbances, makes the sliding mode control technique an efficient tool for this kind of system by making use of the flat outputs. In fact, the differential flatness property of the linear system allows to define a set of new variables which lead to the flat outputs, and therefore, it was possible to parameterize all the states of the linear system in terms of such flat outputs (the attitude angle, the horizontal translational position of the quadrotor, and the oscillation angle of the suspended load). This fact has considerably reduced the complexity of the system resulting in a relatively simple control strategy.

The paper is organized as follows. Section 2 presents the model of a quadrotor with a suspended load and its tangent linearization; the parameterized dynamics based on the flat output is also presented. Section 3 describes the control strategy using the sliding mode technique. In that section, the trajectory tracking error dynamics are formally studied. In Section 4, some simulation results are given making a quantitative comparison of the results obtained with respect to other recent published works related to the same problem. Finally, some conclusions are drawn in Section 5.

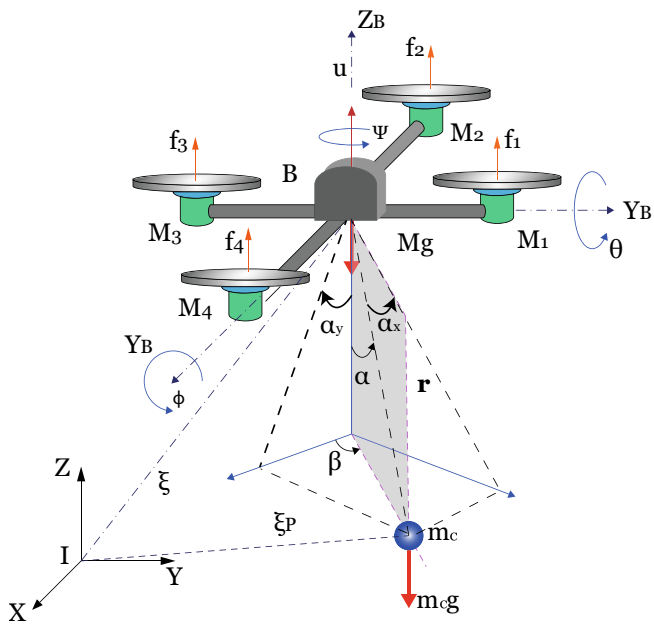


FIGURE 1 The quadrotor with a spherical pendulum. [Color figure can be viewed at [wileyonlinelibrary.com](http://wileyonlinelibrary.com)]

## 2 | MODELING AND TANGENT LINEARIZATION OF THE QUADROTOR WITH A SUSPENDED LOAD

A dynamic model of the quadrotor with slung load is derived in this section. This model is obtained by

$$\mathcal{J} = W_\eta^T \mathcal{I} W_\eta = \begin{bmatrix} I_\phi S_\theta^2 + C_\theta^2(I_\theta S_\phi^2 + I_\psi C_\phi^2) & C_\theta S_\phi C_\phi(I_\theta - I_\psi) & -I_\phi S_\theta \\ C_\theta S_\phi C_\phi(I_\theta - I_\psi) & I_\theta C_\phi^2 + I_\psi S_\phi^2 & 0 \\ -I_\phi S_\theta & 0 & I_\phi \end{bmatrix} \in \mathbb{R}^{3 \times 3}, \quad (6)$$

representing the aircraft as a solid body evolving in a 3D space and subject to the main thrust and three torques as it is shown in Figure 1. The slung load is attached to the geometric center of the quadrotor.

In order to obtain a mathematical model of the system, it is necessary to define a set of reference frames, according to Figure 1:  $\mathbf{I} = \{\mathbf{X}, \mathbf{Y}, \mathbf{Z}\}$  is the inertial frame fixed on earth, and  $\mathbf{B} = \{\mathbf{X}_B, \mathbf{Y}_B, \mathbf{Z}_B\}$  is the body frame fixed in the vehicle. The generalized variables for the system are  $\mathbf{q} = [\xi \eta \mu]^T$ , with  $\mathbf{q} \in \mathbb{R}^8$ , where  $\xi = [x \ y \ z]^T$ , with  $\xi \in \mathbb{R}^3$ ,  $\eta = [\phi \ \theta \ \psi]^T$  where  $\phi, \theta \in (-\pi/2, \pi/2)$  are the Euler angles, with  $\eta \in \mathbb{R}^3$  and  $\mu = [\alpha \ \beta]^T$ , where  $(-\pi/2 < \alpha < \pi/2)$  and  $\mu \in \mathbb{R}^2$  represent the position and orientation of the vehicle and the slung load with respect to the inertial frame.  $M$  and  $m_c$  are the masses of the quadrotor and the load, respectively,  $l$  is the length of the cable from the quadrotor to the payload,  $d$  is the distance among the motors and the center of mass of the quadrotor, while

$f_1, \dots, f_4$  are the thrust forces of each motor. The control inputs are defined as  $\mathbf{u} = [u \ \tau_\phi \ \tau_\theta \ \tau_\psi]^T$ , with  $\mathbf{u} \in \mathbb{R}^4$ , where  $u = f_1 + \dots + f_4$  is the magnitude of the total thrust force and

$$\tau = \begin{bmatrix} \tau_\phi \\ \tau_\theta \\ \tau_\psi \end{bmatrix} = \begin{bmatrix} (f_2 - f_4)d \\ (f_3 - f_1)d \\ \sum_{i=1}^4 \tau_{M_i} \end{bmatrix} \in \mathbb{R}^3 \quad (1)$$

is the generalized torque, which represents the yaw, pitch, and roll moments;  $\tau_{M_i}$  is the moment produced by the motor  $M_i$ .

Let us define the Lagrangian

$$L = K_q + K_p - V, \quad (2)$$

where the kinetic energy of the quadrotor,  $K_q$ , and the kinetic energy of the suspended load,  $K_p$ , are given by

$$K_q = \frac{1}{2} M \dot{\xi}^T \dot{\xi} + \frac{1}{2} \dot{\eta}^T \mathcal{J} \dot{\eta}, \quad (3)$$

$$K_p = \frac{1}{2} m_c \dot{\xi}_p^T \dot{\xi}_p. \quad (4)$$

$V$  is the potential energy of quadrotor and the suspended load; this is

$$V = (M + m_c)gz - m_c g l C_\alpha. \quad (5)$$

The matrix  $\mathcal{J}$  is expressed as

$$\mathcal{J} = \begin{bmatrix} I_\phi & 0 & 0 \\ 0 & I_\theta & 0 \\ 0 & 0 & I_\psi \end{bmatrix} \in \mathbb{R}^{3 \times 3}, \quad (7)$$

and

$$W_\eta = \begin{bmatrix} -S_\theta & 0 & 1 \\ C_\theta S_\phi & C_\phi & 0 \\ C_\theta C_\phi & -C_\phi & 0 \end{bmatrix} \in \mathbb{R}^{3 \times 3}. \quad (8)$$

The position of the suspended load  $\xi_p$ , with respect to the inertial frame  $\mathbf{I}$ , is defined as

$$\xi_p = \xi + l \mathbf{r}, \quad (9)$$

where  $\mathbf{r}$  is the position of the suspended load respect to the inertial body frame  $\mathbf{B}$  defined as  $\mathbf{r} = [S_\alpha \ C_\beta \ S_\alpha \ S_\beta \ C_\alpha]^T \in \mathbb{R}^3$ .

The model of the full quadrotor with slung load is obtained from Euler–Lagrange's equations as

$$\frac{d}{dt} \left( \frac{\partial L}{\partial \dot{\mathbf{q}}} \right) - \frac{\partial L}{\partial \mathbf{q}} = \begin{bmatrix} \mathbf{F} \\ \tau \\ 0 \\ 0 \end{bmatrix} \in \mathbb{R}^8, \quad (10)$$

where  $\mathbf{F} = \mathbf{R}\mathbf{f} \in \mathbb{R}^3$  is the translational force applied to the quadrotor.  $\mathbf{R}$  is the rotation matrix [41] that represents the orientation of the air frame  $\mathbf{B}$  relative to the inertial frame  $\mathbf{I}$  ([41], [42]), and  $\mathbf{f} = [00u]^T$  while the vector  $\tau$  is defined in (1). The equation of motion of the suspended pendulum on a quadrotor can then be expressed in the general form as

$$\mathcal{M}(q)\ddot{q} + C(q, \dot{q})\dot{q} + G(q) = \mathbf{B}_L \mathbf{u}_L, \quad (11)$$

where  $q = [xyz\phi\theta\psi\alpha\beta]^T$  is the generalized coordinates vector and

$$\begin{aligned} \mathcal{M}(q) &= \begin{bmatrix} (M+m_c)\mathbf{I}_{3 \times 3} & \mathbf{0}_{3 \times 3} & \Theta \\ \mathbf{0}_{3 \times 3} & \mathcal{J} & \mathbf{0}_{3 \times 2} \\ \Theta^T & \mathbf{0}_{2 \times 3} & \Phi \end{bmatrix} \in \mathbb{R}^{3 \times 3}, \\ C(\dot{q}, q) &= \begin{bmatrix} \mathbf{0}_{3 \times 3} & \mathbf{0}_{3 \times 3} & \Upsilon \\ \mathbf{0}_{3 \times 3} & \mathbf{0}_{3 \times 3} & \mathbf{0}_{3 \times 2} \\ \mathbf{0}_{2 \times 3} & \mathbf{0}_{2 \times 3} & \Psi \end{bmatrix} \in \mathbb{R}^{3 \times 3}, \\ G(\dot{q}, q) &= \begin{bmatrix} \mathbf{0}_{2 \times 1} \\ g(M+m_c) \\ \mathbf{0}_{3 \times 1} \\ \mathcal{G}_\mu \end{bmatrix} \in \mathbb{R}^8, \quad \mathbf{B}_L = \begin{bmatrix} \mathbf{R}e_3 & \mathbf{0}_{3 \times 3} \\ \mathbf{0}_{3 \times 1} & \mathbf{I}_{3 \times 3} \\ \mathbf{0}_{2 \times 1} & \mathbf{0}_{2 \times 3} \end{bmatrix} \\ &\in \mathbb{R}^{8 \times 4} \quad \mathbf{u}_L = \begin{bmatrix} \mathbf{F} \\ \tau \\ 0 \\ 0 \end{bmatrix} \in \mathbb{R}^8 \end{aligned}$$

with  $\mathbf{I}_{3 \times 3}$  being a three-dimensional unitary matrix,  $e_3 = [001]^T$  and

$$\begin{aligned} \Theta &= m_c l \begin{bmatrix} C_\alpha C_\beta & -S_\alpha S_\beta \\ C_\alpha S_\beta & S_\alpha C_\beta \\ S_\alpha & 0 \end{bmatrix} \in \mathbb{R}^{3 \times 2}, \\ \Phi &= \begin{bmatrix} m_c l^2 & 0 \\ 0 & m_c l^2 S_\alpha^2 \end{bmatrix} \in \mathbb{R}^{2 \times 2}, \quad \mathcal{G}_\mu = \begin{bmatrix} m_c l g S_\alpha \\ 0 \end{bmatrix} \in \mathbb{R}^2, \\ \Upsilon &= m_c l \begin{bmatrix} -(\dot{\alpha} S_\alpha C_\beta + \dot{\beta} C_\alpha S_\beta) & -(\dot{\alpha} C_\alpha S_\beta + \dot{\beta} C_\beta S_\alpha) \\ (\dot{\beta} C_\alpha C_\beta - \dot{\alpha} S_\alpha S_\beta) & (\dot{\alpha} C_\alpha C_\beta - \dot{\beta} S_\alpha S_\beta) \\ \dot{\alpha} C_\alpha & 0 \end{bmatrix} \in \mathbb{R}^{3 \times 2}, \\ \Psi &= m_c l^2 \begin{bmatrix} 0 & -\dot{\beta} S_\alpha C_\alpha \\ \dot{\beta} S_\alpha C_\alpha & \dot{\alpha} S_\alpha C_\alpha \end{bmatrix} \in \mathbb{R}^{2 \times 2}. \end{aligned}$$

After some computations, system (11) can be expressed as<sup>1</sup>

$$\begin{aligned} \ddot{x} &= g_x(\phi, \theta, \psi, \alpha, \beta)u + f_x(\alpha, \beta, \dot{\alpha}, \dot{\beta}), \\ \ddot{y} &= g_y(\phi, \theta, \psi, \alpha, \beta)u + f_y(\alpha, \beta, \dot{\alpha}, \dot{\beta}), \\ \ddot{z} &= g_z(\phi, \theta, \psi, \alpha, \beta)u + f_z(\alpha, \beta, \dot{\alpha}, \dot{\beta}), \end{aligned} \quad (12)$$

$$\begin{aligned} \ddot{\phi} &= \frac{\tau_\phi}{I_\phi}, \\ \ddot{\theta} &= \frac{\tau_\theta}{I_\theta}, \\ \ddot{\psi} &= \frac{\tau_\psi}{I_\psi}, \end{aligned} \quad (13)$$

$$\begin{aligned} \ddot{\alpha} &= g_\alpha(\phi, \theta, \psi, \alpha, \beta)u + f_\alpha(\alpha, \dot{\beta}), \\ \ddot{\beta} &= g_\beta(\phi, \theta, \psi, \alpha, \beta)u + f_\beta(\alpha, \dot{\alpha}, \dot{\beta}), \end{aligned} \quad (14)$$

where

$$\begin{aligned} g_x(\phi, \theta, \psi, \alpha, \beta) &= \frac{(S_\phi S_\psi + C_\phi C_\psi S_\theta)(M + m_c - m_c S_\alpha^2 + m_c S_\alpha^2 S_\beta^2)}{M(M + m_c)} \\ &- \frac{m_c C_\beta S_\beta C_\psi S_\phi - C_\phi S_\psi S_\theta)(C_\alpha^2 - 1)}{M(M + m_c)} \\ &+ \frac{m_c C_\alpha C_\beta C_\phi S_\alpha C_\theta}{M(M + m_c)}, \end{aligned} \quad (15)$$

$$f_x(\alpha, \beta, \dot{\alpha}, \dot{\beta}) = \frac{m_c l C_\beta S_\alpha (\dot{\alpha}^2 - \dot{\beta}^2 C_\alpha^2 + \dot{\beta}^2)}{M + m_c}, \quad (16)$$

$$\begin{aligned} g_y(\phi, \theta, \psi, \alpha, \beta) &= \frac{m_c C_\beta S_\beta (S_\phi S_\psi + C_\phi C_\psi S_\theta)(C_\alpha^2 - 1)}{M(M + m_c)} \\ &- \frac{(C_\psi S_\phi - C_\phi S_\psi S_\theta)(M + m_c - m_c S_\alpha^2 S_\beta^2)}{M(M + m_c)} \\ &+ \frac{m_c C_\alpha C_\phi S_\alpha S_\beta C_\theta}{M(M + m_c)}, \end{aligned} \quad (17)$$

$$f_y(\alpha, \beta, \dot{\alpha}, \dot{\beta}) = \frac{m_c l S_\alpha S_\beta (\dot{\alpha}^2 + \dot{\beta}^2 S_\alpha^2)}{M + m_c}, \quad (18)$$

$$\begin{aligned} g_z(\phi, \theta, \psi, \alpha, \beta) &= \frac{C_\phi C_\theta (m_c S_\alpha^2 + M)}{M(M + m_c)} \\ &+ \frac{m_c C_\alpha C_\beta S_\alpha (S_\phi S_\psi + C_\phi C_\psi S_\theta)}{M(M + m_c)} \\ &- \frac{m_c C_\alpha S_\alpha S_\beta (C_\psi S_\phi - C_\phi S_\psi S_\theta)}{M(M + m_c)}, \end{aligned} \quad (19)$$

$$\begin{aligned} f_z(\alpha, \beta, \dot{\alpha}, \dot{\beta}) &= -\frac{m_c l \dot{\alpha}^2 C_\alpha - m_c l \dot{\beta}^2 C_\alpha^3 + m_c l \dot{\beta}^2 C_\alpha + Mg + gm_c}{M + m_c}, \end{aligned} \quad (20)$$

<sup>1</sup>The computations were carried out using the Maple software. The files associated to these computations can be found at [https://drive.google.com/drive/folders/18bTMIVH\\_S86-gqEysE5eK5u-gCni5-Ez?usp=sharing](https://drive.google.com/drive/folders/18bTMIVH_S86-gqEysE5eK5u-gCni5-Ez?usp=sharing)

$$\begin{aligned} g_\alpha(\phi, \theta, \psi, \alpha, \beta) &= \frac{C_\alpha S_\beta (C_\psi S_\phi - C_\phi S_\psi S_\theta)}{Ml} \\ &- \frac{C_\alpha C_\beta (S_\phi S_\psi + C_\phi C_\psi S_\theta)}{Ml} \\ &- \frac{C_\phi S_\alpha C_\theta}{Ml}, \end{aligned} \quad (21)$$

$$f_\alpha(\alpha, \dot{\beta}) = \frac{\dot{\beta}^2 S_{2\alpha}}{2}, \quad (22)$$

$$\begin{aligned} g_\beta(\phi, \theta, \psi, \alpha, \beta) &= \frac{C_\beta (C_\psi S_\phi - C_\phi S_\psi S_\theta)}{Ml S_\alpha} \\ &+ \frac{S_\beta (S_\phi S_\psi + C_\phi C_\psi S_\theta)}{Ml S_\alpha}, \end{aligned} \quad (23)$$

$$f_\beta(\alpha, \dot{\alpha}, \dot{\beta}) = -\frac{2\dot{\alpha}\dot{\beta}C_\alpha}{S_\alpha}. \quad (24)$$

## 2.1 | Lateral dynamics

To achieve the translation of a suspended load on a quadrotor using a trajectory tracking scheme, it is necessary to control the set of equations given by (11). The following assumptions are introduced in order to simplify the control problem.

**Assumption 1.** The height dynamics and the yaw dynamics are decoupled of the system.

**Assumption 2.** The system is considered to be symmetrical and can be similarly addressed in the  $X$ - $Z$  and the  $Y$ - $Z$  frame [43].

**Assumption 3.** The rotational movements in the Euler angles are  $-\pi/2 < \phi, \theta < \pi/2$ , [19].

Because the quadrotor in three-dimensional space is reduced to dynamics restricted to two dimensions, the dynamics in altitude and yaw can be considered decoupled from the entire system. Under Assumption 1, the restricted movement with respect to the  $X$ - $Z$  frame can be considered as  $y = \phi = \psi = \beta = 0$  and  $\alpha_y = \arctan 2(S_\alpha C_\beta / C_\alpha)$ . Similarly, for the  $Y$ - $Z$  frame, the restricted movement can be considered as  $x = \theta = \psi = 0$ ,  $\alpha_x = \arctan 2(S_\alpha S_\beta / C_\alpha)$  and  $\beta = -\pi/2$ .

Also, from Assumption 3, the Euler angles can be considered small around of an operating point; this fact allows us to consider a tangent linearization in each dynamics frame. For instance, the equilibrium point associated to the  $X$ - $Z$  frame can be chosen as  $(x(t), z(t), \theta(t), \alpha_x(t)) = (\bar{x}, \bar{z}, 0, 0)$  for  $u(t) = \bar{u} = (M + m_c)g$  and  $\tau_\theta = 0$ , with  $\bar{x}$  and  $\bar{z}$  being positive real constants. The tangent linearized model can then be written as in the  $X$ - $Z$  frame as

$$\ddot{x}_\delta = \frac{(M + m_c)g\theta_\delta - m_c g l \alpha}{M}, \quad (25)$$

$$\ddot{z}_\delta = \frac{u_\delta}{M + m_c}, \quad (26)$$

$$\ddot{\theta}_\delta = \frac{\tau_{\theta_\delta}}{I_\theta}, \quad (27)$$

$$\ddot{\alpha}_{y\delta} = \frac{(M + m_c)g\theta_\delta - (M + m_c)g\alpha_\delta}{Ml}, \quad (28)$$

where  $x_\delta = x - \bar{x}$ ,  $z_\delta = z - \bar{z}$ ,  $\theta_\delta = \theta - 0$  and  $\alpha_{y\delta} = \alpha_y - 0$  are deviation variables.

For the  $Y$ - $Z$  frame, the equilibrium point is chosen as  $(y(t), z(t), \phi(t), \alpha_y(t)) = (\bar{y}, \bar{z}, 0, 0)$  for  $u(t) = \bar{u} = (M + m_c)g$ , and  $\tau_\phi = 0$ , with  $\bar{y}$  and  $\bar{z}$  being positive real constants. Thus, the tangent linearized model can also be written in the  $Y$ - $Z$  frame as

$$\ddot{y}_\delta = \frac{m_c g l \alpha - (M + m_c)g\phi_\delta}{M}, \quad (29)$$

$$\ddot{z}_\delta = \frac{u_\delta}{M + m_c}, \quad (30)$$

$$\ddot{\phi}_\delta = \frac{\tau_{\phi_\delta}}{I_\phi}, \quad (31)$$

$$\ddot{\alpha}_{x\delta} = \frac{(M + m_c)g\phi_\delta - (M + m_c)g\alpha_\delta}{Ml}, \quad (32)$$

where  $y_\delta = y - \bar{y}$ ,  $\phi_\delta = \phi - 0$ , and  $\alpha_{x\delta} = \alpha_x - 0$  are also deviation variables.

## 2.2 | The flat outputs

A system is differentially flat if there exists a set of so-called flat outputs, such that the state and inputs of the system can be expressed as smooth functions of the flat outputs and their higher-order derivative [40, 44]. In this case, we can choose the flat outputs in each frame as

$$\mathcal{L} = z_\delta, \quad (33)$$

$$\mathcal{F}_x = x_\delta - l\alpha_\delta, \quad (34)$$

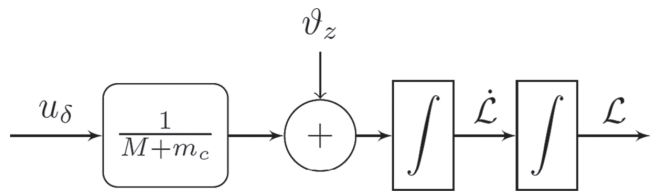
$$\mathcal{F}_y = y_\delta + l\alpha_\delta. \quad (35)$$

All variables can be parameterized in terms of  $\mathcal{F}_x$ ,  $\mathcal{F}_y$ , and  $\mathcal{L}$  and a finite number of its time derivatives. The  $\mathcal{L}$  variable is parameterized in terms of the variables associated with the vertical dynamics; this is the  $z$  dynamics, more precisely,

$$z_\delta = \mathcal{L}, \quad (36)$$

$$\dot{z}_\delta = \dot{\mathcal{L}}, \quad (37)$$

$$f_\delta = (M + m_c)\ddot{\mathcal{L}}. \quad (38)$$

FIGURE 2 Flat output's cascade representation  $\mathcal{L}$ .

The flat output  $\mathcal{L}$  (equation (33)) and its time derivatives exhibit the following relations:

$$\mathcal{L} = z_\delta, \quad (39)$$

$$\dot{\mathcal{L}} = \dot{z}_\delta, \quad (40)$$

$$\ddot{\mathcal{L}} = \frac{f_\delta}{M + m_c}. \quad (41)$$

In a similar way,  $\mathcal{F}_x$  and  $\mathcal{F}_y$  are parameterized in terms of all variables of the linear system associated with the horizontal motion in the  $X$ - $Z$  frame (see Martinez-Vasquez et al. [45] for more details),

Thus,  $\mathcal{F}_x$  and its sixth time derivative exhibit the following relation:

$$\mathcal{F}_x^{(6)} = \frac{g^2(M + m_c)}{I_\theta M l} \tau_{\theta_\delta} - \frac{g(M + m_c)}{M l} \mathcal{F}_x^{(4)}. \quad (42)$$

In a similar way,  $\mathcal{F}_y$  and its sixth time derivative take the form

$$\mathcal{F}_y^{(6)} = -\frac{g^2(M + m_c)}{I_\phi M l} \tau_{\phi_\delta} - \frac{g(M + m_c)}{M l} \mathcal{F}_y^{(4)}. \quad (43)$$

In Figures 2–4, the cascade representation of the flats outputs  $\mathcal{L}$ ,  $\mathcal{F}_x$ , and  $\mathcal{F}_y$  is shown. In these diagrams, the disturbances  $\vartheta_x$  and  $\vartheta_z$  are added, which represent the nonlinearities neglected in the linearization process, as well as any other external disturbances.

### 3 | CONTROL STRATEGIES

In this section, the control strategies for stabilizing and controlling the quadrotor and the oscillation of the suspended load, using the flatness concept and the sliding mode technique, are presented. The objective is to control the system in the height  $z$  and the yaw  $\psi$  angle by means of the control input  $u$  and  $\tau_\psi$ , reaching a smooth desired path. In the same way, a smooth desired path is assigned to the flat outputs  $\mathcal{F}_x$  and  $\mathcal{F}_y$ , in the  $X$ - $Y$  and  $Y$ - $Z$  frames, through the inputs  $\tau_\phi$  and  $\tau_\theta$ . Since the disturbances  $\vartheta_x(t)$ ,  $\vartheta_y(t)$ ,  $\vartheta_z(t)$ , and  $\vartheta_\psi(t)$  are introduced to the system, the following assumption is made.

**Assumption 4.** The disturbances  $\vartheta_x(t)$ ,  $\vartheta_y(t)$ ,  $\vartheta_z(t)$ , and  $\vartheta_\psi(t)$  are bounded. This is

$$\|\vartheta_i(t)\| \leq \bar{\vartheta}_i, \quad (44)$$

where  $\bar{\vartheta}_i$  is a nonzero positive finite real number and  $i = x, y, \psi, z$ .

All the maneuvers of the quadrotor must be executed, while the suspended load evolves close to its equilibrium point, so that trajectory following errors  $e_z = z - z_d$ ,  $e_\psi = \psi - \psi_d$ ,  $e_{\mathcal{F}_x} = \mathcal{F}_x - F_{y_d}$ , and  $e_{\mathcal{F}_y} = \mathcal{F}_y - F_{y_d}$  remain bounded.

#### 3.1 | Height and yaw control

Since the height and the yaw dynamics correspond to a second-order system, let us consider a generalized second-order differential system, based on the third equation in (12) and (13), of the form

$$\ddot{\mathcal{Y}} = \mathcal{U} + \vartheta(t), \quad (45)$$

where  $\mathcal{U}$  and  $\vartheta(t)$  can be  $\mathcal{Y} = z$ ,  $\mathcal{U} = g_z(\phi, \theta, \psi, \alpha, \beta)u$ , and  $\vartheta(t) = \vartheta_z(t) + f_z(\alpha, \beta, \dot{\alpha}, \dot{\beta})$  for the case of the height dynamics or  $\mathcal{Y} = \psi$ ,  $\mathcal{U} = \tau_\psi/I_\psi$ , and  $\vartheta(t) = \vartheta_\psi(t)$  for the case of the yaw dynamics; thus,  $\vartheta(t)$  is a term that contains unknown external disturbances such as wind gusts and other perturbations. The trajectory tracking errors are defined as  $e_y = \mathcal{Y} - \mathcal{Y}^*(t)$  and  $e_U = \mathcal{U} - \mathcal{U}^*$ , being  $\mathcal{Y}^*(t)$  the desired trajectory which is assumed to be  $C^\infty$  and  $\mathcal{U}^* = \ddot{\mathcal{Y}}^*(t)$ . System (45) can be written in terms of the tracking error  $e_y$  as

$$\ddot{e}_y = e_U + \vartheta(t). \quad (46)$$

The main idea of the sliding mode control is to modify the dynamics of the system by applying a discontinuous feedback control input that forces the system to slide over a predefined surface and the system produces the desired behavior by constraining its state to evolve on this surface. This sliding surface is selected by means of a switching function given by

$$s = \dot{e}_y(t) + \mu_1 e_y(t) + \mu_0 \int_0^t e_y(\varpi) d\varpi, \quad (47)$$

where  $\mu_0$  and  $\mu_1$  are positive real coefficients different from zero.

If the states of the system (45) are forced to slide over the sliding function  $s = 0$ , then  $e_y$  asymptotically converges to the origin. A Lyapunov function is proposed in order to design a feedback that allows to attain this surface [46]. The following Lyapunov function is proposed:

$$V_{hy} = \frac{1}{2}s^2, \quad (48)$$

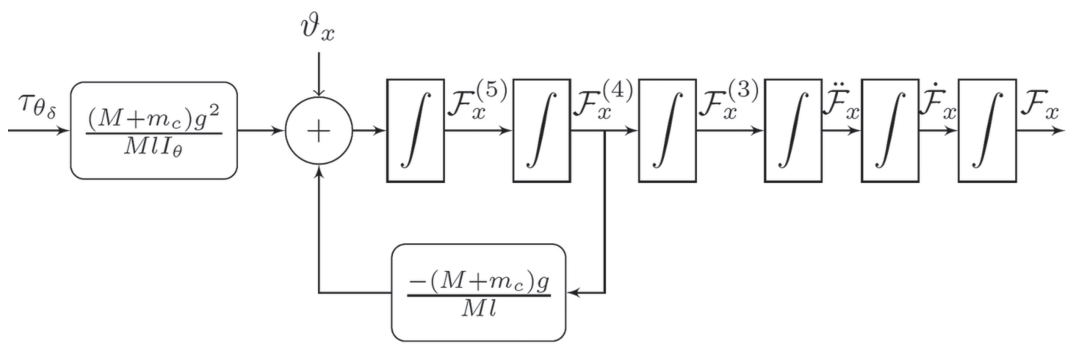


FIGURE 3 Cascade representation of the flat output  $\mathcal{F}_x$ .

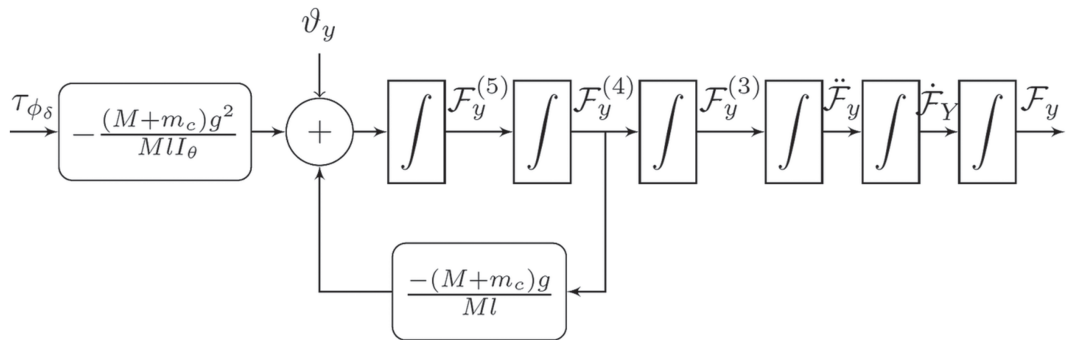


FIGURE 4 Cascade representation of the flat output  $\mathcal{F}_y$ .

whose time derivative, when substituting the dynamics (46), takes the form

$$\dot{V}_{hy} = s(e_U + \vartheta(t) + \mu_1 \dot{e}_Y + \mu_0 e_Y). \quad (49)$$

If  $\dot{V}_{hy} < 0$ , the trajectories of (46) attain the surface  $s = 0$ . Consider the feedback

$$e_U = -\mu_1 \dot{e}_Y - \mu_0 e_Y - \rho \cdot \text{sign}(s), \quad (50)$$

with  $\mu_0 = \lambda_0 > 0$ ,  $\mu_1 = \lambda_1 > 0$ ,  $\rho = \rho_z > 0$ , when  $U = z$  and  $\mu_0 = \gamma_0 > 0$ ,  $\mu_1 = \gamma_1 > 0$ ,  $\rho = \rho_\psi > 0$ , when  $U = \psi$ .  $\text{sign}(s)$  is the signum function defined as

$$\text{sign}(s) = \begin{cases} +1 & \text{if } s > 0 \\ -1 & \text{if } s < 0. \end{cases} \quad (51)$$

Since  $s \cdot \text{sign}(s) = |s|$  one has that, together with Assumption 4,

$$\dot{V}_{hy} = -\rho|s| + s\vartheta(t) \leq -|s|(\rho - \bar{\vartheta}), \quad (52)$$

where  $\bar{\vartheta}$  is either  $\bar{\vartheta}_z$  or  $\bar{\vartheta}_\psi$ . For  $\rho > \bar{\vartheta}$ ,  $\dot{V}_{hy} < 0$ ; therefore, the trajectories of system (46) will reach the surface  $s = 0$  [46]. If

$$\rho - \bar{\vartheta} \geq \rho_0 > 0, \quad (53)$$

with  $\rho_0$  being a positive real constant, one has that

$$\dot{V}_{hy} \leq -\rho_0|s|, \quad (54)$$

and since  $V_{hy} = \frac{1}{2}s^2 = \frac{1}{2}|s|^2$ ,  $|s| = \sqrt{2V_{hy}}$  leads to

$$\dot{V}_{hy} \leq -\eta V_{hy}^{\frac{1}{2}}, \quad (55)$$

with  $\eta = \rho_0\sqrt{2}$ . Consider now the scalar differential function

$$\dot{v}_{hy} = -\eta v_h^{\frac{1}{2}} y(t) \quad (56)$$

with  $v_{hy}(0) = v_{hy,0}$  and its solution

$$v_{hy}(t) = \left( -\frac{\eta}{2}t + \sqrt{v_{hy,0}} \right)^2, \quad (57)$$

Since  $V_{hy}$  is a continuous function which is differentiable at  $t$  that satisfies the differential inequality (55), one has from the comparison lemma (see Khalil [47], chapter 3, section 3.4) that

$$V_{hy}(t) \leq \left( -\frac{\eta}{2}t + \sqrt{V_{hy,0}} \right)^2, \quad (58)$$

with  $V_{hy,0} = V_{hy}(0)$ . Then, since the solution vanishes after some

$$t_s \leq \frac{2}{\eta} \sqrt{V_{hy,0}}, \quad (59)$$

$s$  vanishes as well and the sliding mode starts after a finite time interval. From (46) and (50), it follows that the control which achieves height trajectory tracking is given by

$$u = \frac{\ddot{z}^*(t) - \lambda_1 \dot{e}_z - \lambda_0 e_z - \rho_z \cdot \text{sign}(s)}{g_z(\phi, \theta, \psi, \alpha, \beta)}. \quad (60)$$

Following the same reasoning, the control that achieves yaw trajectory tracking is given by

$$\tau_\psi = I_\psi(\ddot{\psi}^*(t) - \gamma_1 \dot{e}_\psi - \gamma_0 e_\psi - \rho_\psi \cdot \text{sign}(s)). \quad (61)$$

### 3.2 | Horizontal control

The horizontal control is carried out in the  $X$ - $Z$  and  $Y$ - $Z$  frames, by means the control inputs  $\tau_\phi$  and  $\tau_\theta$ , and it has three fundamental tasks:

1. To stabilize the rotational dynamics, this is the Euler angles  $\theta$  (pitch) and  $\phi$  (roll).
2. To follow a desired trajectory in the translational dynamics.
3. To maintain the minimum oscillation of the suspended load ( $\alpha$  angle).

These tasks are carried out through the parameterization of the system using the flat outputs given by expressions (42) and (43). In order to reduce the design process, and due the fact that both controls have a similar structure, we define a generalized sixth-order differential equation, with an added external disturbance term, in the form

$$\mathcal{F}^{(6)} = u_F + \vartheta(t), \quad (62)$$

where  $\mathcal{F} = \mathcal{F}_x$ ,  $u_F = \frac{g^2(M+m_c)}{MI_\theta} \tau_{\theta_\delta} - \frac{g(M+m_c)}{MI} \mathcal{F}_x^{(4)}$ ,  $\vartheta(t) = \vartheta_x(t)$  for the dynamics in the frame  $X$  –  $Z$ , or  $\mathcal{F} = \mathcal{F}_y$ ,  $u_F = -\frac{g^2(M+m_c)}{MI_\phi} \tau_{\phi_\delta} - \frac{g(M+m_c)}{MI} \mathcal{F}_y^{(4)}$ ,  $\vartheta(t) = \vartheta_y(t)$  for the dynamics in the  $Y$  –  $Z$  frame. In order to develop a trajectory tracking control, the error is defined as  $e_F = \mathcal{F} - \mathcal{F}^*(t)$ , where  $\mathcal{F}^*(t)$  is the desired trajectory in each frame, this is  $\mathcal{F}_x^*(t)$  or  $\mathcal{F}_y^*(t)$  for the desired trajectory along the  $X$  axis or  $Y$  axis, respectively. These trajectory references are supposed to be  $C^\infty$ , together with  $e_{uF} = u_F - u_F^*$  where  $u_F^* = \mathcal{F}^*(t)^{(6)}$ . Then, the dynamics of the tracking error  $e_F$  can be expressed as

$$e_F^{(6)} = e_{uF}(t) + \vartheta(t). \quad (63)$$

Applying the same methodology described above for the computation of the height and yaw controls, a switching function is proposed as

$$\begin{aligned} \sigma = & e_F^{(5)}(t) + \mathcal{K}_5 e_F^{(4)}(t) + \mathcal{K}_4 e_F^{(3)}(t) + \mathcal{K}_3 e_F^{(2)}(t) + \mathcal{K}_2 e_F^{(1)}(t) \\ & + \mathcal{K}_1 e_F(t) + \mathcal{K}_0 \int_0^t e_F(\varpi) d\varpi, \end{aligned} \quad (64)$$

where  $\mathcal{K}_5, \mathcal{K}_4, \mathcal{K}_3, \mathcal{K}_2, \mathcal{K}_1$ , and  $\mathcal{K}_0$  are positive real coefficients different from zero chosen in such a way that, if all variables of the corresponding dynamics are restricted to the sliding surface  $\sigma = 0$ , the trajectory tracking error  $e_F$  goes to zero asymptotically.

In order to attract the dynamics variables to  $\sigma = 0$ , a horizontal control can be obtained by means of the Lyapunov function

$$V_F = \frac{1}{2} \sigma^2, \quad (65)$$

whose time derivative along the dynamics (63) takes the form

$$\begin{aligned} \dot{V}_F = & \sigma(e_{uF} + \vartheta(t) + \mathcal{K}_5 e_F^{(5)} + \mathcal{K}_4 e_F^{(4)} + \mathcal{K}_3 e_F^{(3)} \\ & + \mathcal{K}_2 e_F^{(2)} + \mathcal{K}_1 e_F^{(1)} + \mathcal{K}_0 e_F). \end{aligned} \quad (66)$$

Let us choose the feedback

$$\begin{aligned} e_{uF} = & -\mathcal{K}_5 e_F^{(5)} - \mathcal{K}_4 e_F^{(4)} - \mathcal{K}_3 e_F^{(3)} - \mathcal{K}_2 e_F^{(2)} - \mathcal{K}_1 e_F^{(1)} \\ & - \mathcal{K}_0 e_F - \rho_F \cdot \text{sign}(\sigma), \end{aligned} \quad (67)$$

with  $\rho_F > 0$  and  $\text{sign}(\sigma)$  being the signum function defined before. Using again the fact that  $\sigma \cdot \text{sign}(\sigma) = |\sigma|$ , one has that, together with Assumption 4,

$$\dot{V}_F = -\rho_F |\sigma| + \sigma \vartheta(t) \leq -|\sigma|(\rho_F - \bar{\vartheta}), \quad (68)$$

For  $\rho_F > \bar{\vartheta}$ ,  $\dot{V}_F < 0$ ; therefore, all trajectories of system (63) attain the sliding surface  $\sigma = 0$  [46]. If

$$\rho_F - \bar{\vartheta} \geq \rho_{F0} > 0, \quad (69)$$

with  $\rho_{F0}$  being a positive real constant, one has that

$$\dot{V}_F \leq -\rho_{F0} |s|, \quad (70)$$

and since  $V_F = \frac{1}{2} \sigma^2 = \frac{1}{2} |\sigma|^2$ ,  $|\sigma| = \sqrt{2V_F}$  leads again to

$$\dot{V}_F \leq -\eta V_F^{\frac{1}{2}}, \quad (71)$$

with  $\eta = \rho_{F0} \sqrt{2}$ .

The solution of this last expression is, as before, nonnegative and is bounded by

$$V_F(t) \leq \left( -\frac{\eta}{2} t + \sqrt{V_{F,0}} \right)^2, \quad (72)$$

with  $V_{F,0} = V_F(0)$ . Then, since the solution vanishes after some  $t_s \leq \frac{2}{\eta} \sqrt{V_{F,0}}$ ,  $\sigma$  vanishes as well and the sliding mode starts after a finite time interval.

From (67), one obtains the sliding mode control that allows to have attitude trajectory tracking in system (62);

this is

$$\begin{aligned} u_F = & \mathcal{F}^{*(6)} - \mathcal{K}_5 e_F^{(5)} - \mathcal{K}_4 e_F^{(4)} - \mathcal{K}_3 e_F^{(3)} - \mathcal{K}_2 e_F^{(2)} - \mathcal{K}_1 e_F^{(1)} \\ & - \mathcal{K}_0 e_F - \rho_F \cdot \text{sign}(\sigma). \end{aligned} \quad (73)$$

Thus, the sliding mode control law that allows to have trajectory tracking of the quadrotor transporting a suspended load with minimum oscillations along the  $X$ - $Z$  frame is given by

$$\begin{aligned} \tau_\theta = & \frac{MlI_\theta}{g^2(M+m_c)} \{ \mathcal{F}_x^{*(6)} - \mathcal{K}_5(\mathcal{F}_x^{(5)} - \mathcal{F}_x^{*(5)}) \\ & - \mathcal{K}_4(\mathcal{F}_x^{(4)} - \mathcal{F}_x^{*(4)}) - \mathcal{K}_3(\mathcal{F}_x^{(3)} - \mathcal{F}_x^{*(3)}) - \mathcal{K}_2(\ddot{\mathcal{F}}_x - \ddot{\mathcal{F}}_x^*) \\ & - \mathcal{K}_1(\dot{\mathcal{F}}_x - \dot{\mathcal{F}}_x^*) - \mathcal{K}_0(\mathcal{F}_x - \mathcal{F}_x^*) \\ & - \rho_{F_x} \cdot \text{sign}(\sigma) \} + \frac{I_\theta}{g} \mathcal{F}_x^{(4)}. \end{aligned} \quad (74)$$

In a similar way, the sliding mode control law in the  $Y$ - $Z$  frame is given by

$$\begin{aligned} \tau_\phi = & -\frac{MlI_\phi}{g^2(M+m_c)} \{ \mathcal{F}_y^{*(6)} - \mathcal{K}_5(\mathcal{F}_y^{(5)} - \mathcal{F}_y^{*(5)}) \\ & - \mathcal{K}_4(\mathcal{F}_y^{(4)} - \mathcal{F}_y^{*(4)}) - \mathcal{K}_3(\mathcal{F}_y^{(3)} - \mathcal{F}_y^{*(3)}) - \mathcal{K}_2(\ddot{\mathcal{F}}_y - \ddot{\mathcal{F}}_y^*) \\ & - \mathcal{K}_1(\dot{\mathcal{F}}_y - \dot{\mathcal{F}}_y^*) - \mathcal{K}_0(\mathcal{F}_y - \mathcal{F}_y^*) \\ & - \rho_{F_y} \cdot \text{sign}(\sigma) \} - \frac{I_\phi}{g} \mathcal{F}_y^{(4)}. \end{aligned} \quad (75)$$

### 3.3 | Tracking error stability analysis

Based on the control structures developed in subsections 3.1 and 3.2, one can study the tracking error behavior of the closed loop system. One has the following result.

**Theorem 1.** Consider the controllers given by equations (60), (61), (74), and (75), together with Assumptions 1–4. Then, the trajectories of the tracking errors  $e_z$ ,  $e_\psi$ ,  $e_{F_x}$ ,  $e_{F_y}$  and their time derivatives converge globally towards a sphere of radius as small as desired provided that the constants coefficients  $\lambda_0$ ,  $\lambda_1$ ,  $\gamma_0$ ,  $\gamma_1$ ,  $\mathcal{K}_0$ ,  $\mathcal{K}_1$ ,  $\mathcal{K}_2$ ,  $\mathcal{K}_3$ ,  $\mathcal{K}_4$ , and  $\mathcal{K}_5$  in the polynomials

$$\begin{aligned} q_1(p) &= p^2 + \lambda_1 p + \lambda_0, \\ q_2(p) &= p^2 + \gamma_1 p + \gamma_0, \\ q_3(p) &= p^6 + \mathcal{K}_5 p^5 + \mathcal{K}_4 p^4 + \mathcal{K}_3 p^3 + \mathcal{K}_2 p^2 + \mathcal{K}_1 p + \mathcal{K}_0, \end{aligned} \quad (76)$$

are chosen so that, for a sufficient number  $\mathcal{N} > 0$ ,  $q_1(p)$ ,  $q_2(p)$  and  $q_3(p)$  exhibit all their roots to the left of the line  $\{p \in \mathbb{C} \mid \text{Re}(p) \leq -\mathcal{N}\}$  in the complex plane  $\mathbb{C}$ .

*Proof.* Let  $\mathbf{e}_x$  denote the trajectory tracking errors and their time derivatives; this is  $\mathbf{e}_x = (e_z \dot{e}_z)^T$  or  $\mathbf{e}_x =$

$(e_\psi \dot{e}_\psi)^T$  for the height and yaw dynamics and  $\mathbf{e}_x = (e_F \dot{e}_F^{(1)} \dot{e}_F^{(2)} \dot{e}_F^{(3)} \dot{e}_F^{(4)} \dot{e}_F^{(5)})^T$  for the horizontal dynamics represented by the parameterization of the flat outputs, where  $e_F$  can be either  $e_{F_x}$  or  $e_{F_y}$ .  $\vartheta(t)$  represents the disturbances. Then, the closed-loop system tracking error dynamics can be rewritten in a generalized form as

$$\dot{\mathbf{e}}_x = \mathbf{A}_e \mathbf{e}_x + \mathbf{b}_e (R_e(\mathbf{e}_x) + \vartheta(t)), \quad (77)$$

where

$$\mathbf{A}_e = \begin{bmatrix} 0 & 1 \\ -\lambda_0 & -\lambda_1 \end{bmatrix}, \quad \mathbf{b}_e = \begin{bmatrix} 0 \\ 1 \end{bmatrix}, \quad R_e(\mathbf{e}_x) = -\rho_z \cdot \text{sign}(s) \quad (78)$$

for the height tracking error dynamics,

$$\mathbf{A}_e = \begin{bmatrix} 0 & 1 \\ -\gamma_0 & -\gamma_1 \end{bmatrix}, \quad \mathbf{b}_e = \begin{bmatrix} 0 \\ 1 \end{bmatrix}, \quad R_e(\mathbf{e}_x) = -\rho_\psi \cdot \text{sign}(s) \quad (79)$$

for the yaw tracking error dynamics, and

$$\begin{aligned} \mathbf{A}_e = & \begin{bmatrix} 0 & 1 & 0 & 0 & 0 & 0 \\ 0 & 0 & 1 & 0 & 0 & 0 \\ 0 & 0 & 0 & 1 & 0 & 0 \\ 0 & 0 & 0 & 0 & 1 & 0 \\ 0 & 0 & 0 & 0 & 0 & 1 \\ -\mathcal{K}_0 & -\mathcal{K}_1 & -\mathcal{K}_2 & -\mathcal{K}_3 & -\mathcal{K}_4 & -\mathcal{K}_5 \end{bmatrix}, \\ \mathbf{b}_e = & \begin{bmatrix} 0 \\ 0 \\ 0 \\ 0 \\ 0 \\ 1 \end{bmatrix}, \quad R_e(\mathbf{e}_x) = -\rho_F \cdot \text{sign}(\sigma) \end{aligned} \quad (80)$$

for the horizontal tracking error dynamics, where  $\mathcal{F}$  is either  $\mathcal{F}_x$  or  $\mathcal{F}_y$ .

Since the matrix  $\mathbf{A}_e$  in (78)–(80) is Hurwitz, there exists a real symmetric positive definite matrix  $P_e$  which is a solution of the Lyapunov equation

$$P_e \mathbf{A}_e + \mathbf{A}_e^T P_e = -Q_e, \quad (81)$$

for a given real symmetric positive definite matrix  $Q_e$ . The following Lyapunov is then considered

$$V_e = \frac{1}{2} \mathbf{e}_x^T P_e \mathbf{e}_x, \quad (82)$$

whose time derivative along the dynamics (77) is given by

$$\dot{V}_e = -\mathbf{e}_x^T Q_e \mathbf{e}_x + 2\mathbf{e}_x^T P_e b_e [-\rho \cdot \text{sign}(\nu) + \vartheta(t)], \quad (83)$$

where  $\nu$  is either  $s$  or  $\sigma$ . Notice that  $\mathbf{e}_x^T Q_e \mathbf{e}_x \geq \lambda_{\min}(Q_e) \|\mathbf{e}_x\|^2$  where  $\lambda_{\min}(Q_e)$  denotes the minimum eigenvalue of matrix  $Q_e$  and since  $Q_e$  is symmetric and positive definite, then  $\lambda_{\min}(Q_e)$  is real and positive. From this, together with Assumption 4, and taking into

TABLE 1 Model simulation parameters.

| Parameter                             | Value (unit)             |
|---------------------------------------|--------------------------|
| Mass of the quadrotor, ( $M$ )        | 0.5 (kg)                 |
| Mass of the suspended load, ( $m_c$ ) | 0.2 (kg)                 |
| Cable length, ( $l$ )                 | 0.3 (m)                  |
| Gravitational acceleration, ( $g$ )   | 9.8 (m/s <sup>2</sup> )  |
| Inertia ( $I_\phi$ )                  | 0.1 (kg.m <sup>2</sup> ) |
| Inertia, ( $I_\theta$ )               | 0.1 (kg.m <sup>2</sup> ) |
| Inertia, ( $I_\psi$ )                 | 0.1 (kg.m <sup>2</sup> ) |

account the fact that  $\|\rho \cdot \text{sign}(s)\| \leq \rho$ , with  $\rho = \rho_z$  or  $\rho = \rho_\psi$ , and  $\|\rho \cdot \text{sign}(\sigma)\| \leq \rho$ , with  $\rho = \rho_F$ , one has that

$$\dot{V}_e \leq -\lambda_{\min}(Q_e) \|\mathbf{e}_x\| \left( \|\mathbf{e}_x\| - \frac{2\|P_e \mathbf{b}_e\|(\rho + \bar{\vartheta})}{\lambda_{\min}(Q_e)} \right). \quad (84)$$

Then, for

$$\|\mathbf{e}_x\| > \frac{2\|P_e \mathbf{b}_e\|(\rho + \bar{\vartheta})}{\lambda_{\min}(Q_e)}, \quad (85)$$

$\dot{V}_e < 0$  and the tracking error dynamics  $\mathbf{e}_x$  has convergence to a ball defined as

$$S(0, \rho) = \left\{ \|\mathbf{e}_x\| \in \mathbb{R}^n : \|\mathbf{e}_x\| < \frac{2\|P_e \mathbf{b}_e\|(\rho + \bar{\vartheta})}{\lambda_{\min}(Q_e)} \right\}. \quad (86)$$

If

$$\|\mathbf{e}_x\| \geq \frac{2\|P_e \mathbf{b}_e\|(\rho + \bar{\vartheta})}{\lambda_{\min}(Q_e)} + \rho_{0e} > 0, \quad (87)$$

where  $\rho_{0e}$  is a positive real constant, one has that

$$\dot{V}_e \leq -\lambda_{\min}(Q_e) \|\mathbf{e}_x\| \rho_{0e}. \quad (88)$$

Since  $V_e = \frac{1}{2} \mathbf{e}_x^T P_e \mathbf{e}_x$ , then  $\frac{V_e}{\|\mathbf{e}_x\|} \leq \frac{1}{2} \|\mathbf{e}_x\| \|P_e\|$  and  $\frac{\mathbf{e}_x}{\|\mathbf{e}_x\|} = \frac{1}{2} \|\mathbf{e}_x\| \|P_e\|$ , or equivalently,  $\|\mathbf{e}_x\| \geq \sqrt{\frac{2}{\|P_e\|}} V_e^{\frac{1}{2}}$ ; thus, (88) can be reiterated as

$$\dot{V}_e \leq -\eta_e V_e^{\frac{1}{2}}, \quad (89)$$

where  $\eta_e = \lambda_{\min}(Q_e) \sqrt{\frac{2}{\|P_e\|}}$ . As before, the solution of (89) is nonnegative and is bounded by

$$V_e(t) \leq \left( -\frac{\eta_e}{2} t + \sqrt{V_{e,0}} \right)^2, \quad (90)$$

where  $V_{e,0} = V_e(0)$ . Thus, since the solution of (89) vanishes after some

$$t_{s,e} < \frac{2}{\eta_e} \sqrt{V_{e,0}}, \quad (91)$$

$\mathbf{e}_x$  enters the ball  $S(0, \rho)$  after a finite time interval and all trajectories starting inside this ball do not leave it.  $\square$

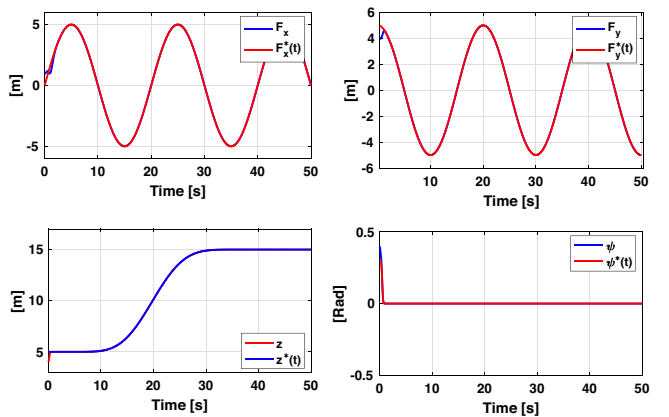


FIGURE 5 Trajectory tracking of  $F_x$ ,  $F_y$ ,  $z$ , and  $\psi$ . [Color figure can be viewed at wileyonlinelibrary.com]

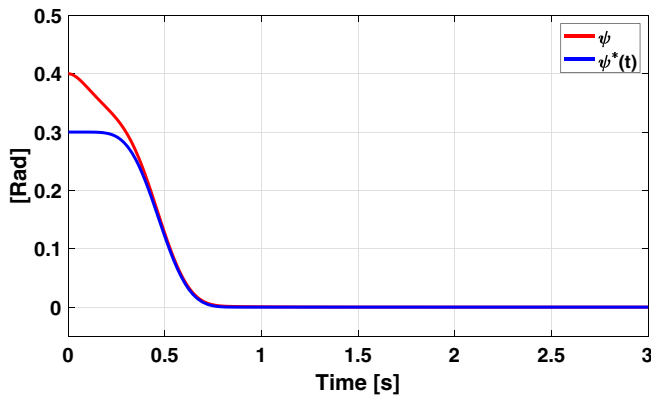


FIGURE 6 Trajectory tracking of the yaw angle  $\psi$  for the first 3 s simulation. [Color figure can be viewed at wileyonlinelibrary.com]

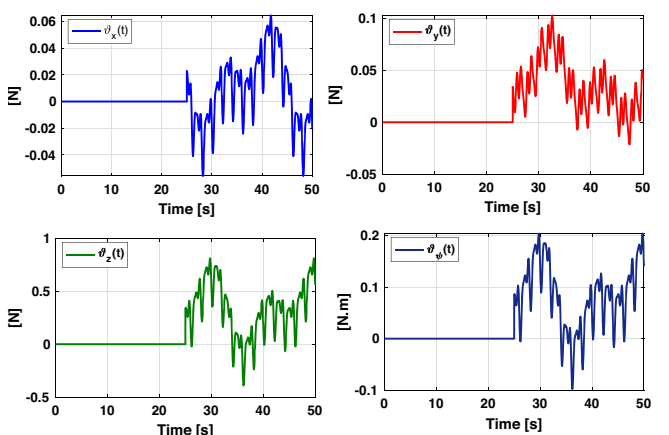


FIGURE 7 External disturbances  $\theta_x(t)$ ,  $\theta_y(t)$ ,  $\theta_z(t)$ , and  $\theta_\psi(t)$ . [Color figure can be viewed at wileyonlinelibrary.com]

*Remark 1.* It is worthwhile to notice that the larger the quantity  $\lambda_{\min}(Q_e)$  is, the smaller the radius of the ultimate bounding ball  $S(0, \rho)$  is.

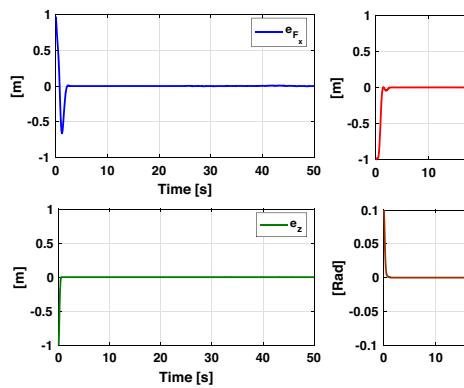
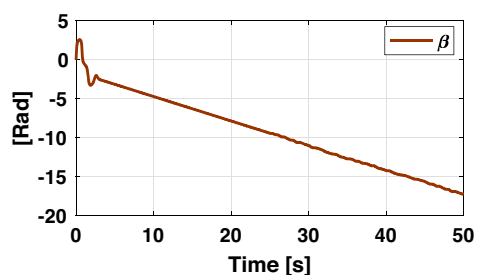
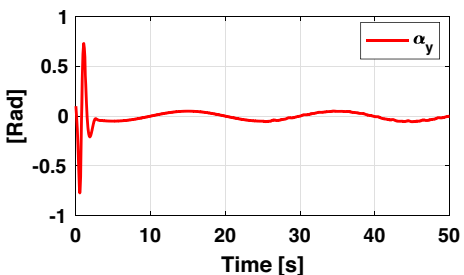
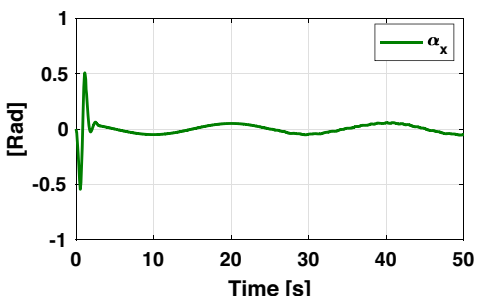
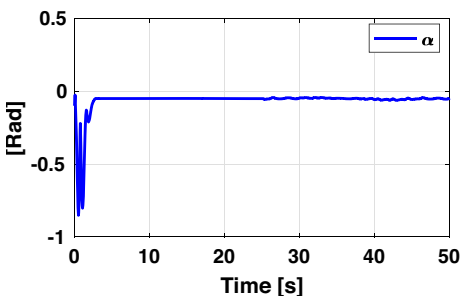


FIGURE 9 Trajectory tracking errors  $e_{F_x}$ ,  $e_{F_y}$ ,  $e_z$ , and  $e_y$ . [Color figure can be viewed at wileyonlinelibrary.com]

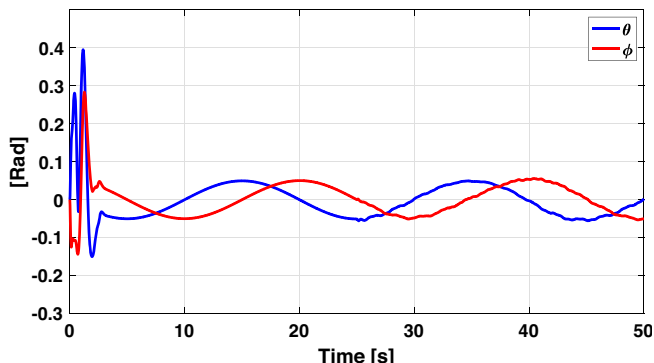
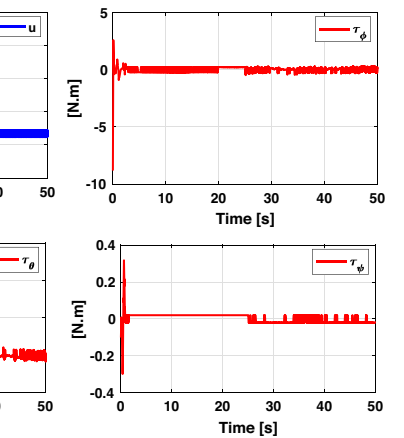
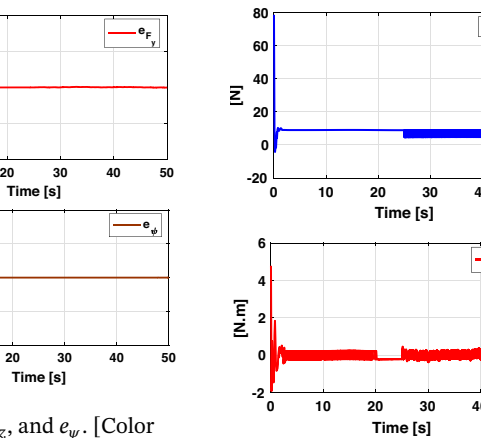


FIGURE 10 Attitude angles  $\phi$  and  $\theta$ . [Color figure can be viewed at wileyonlinelibrary.com]

## 4 | SIMULATIONS RESULTS

Numerical simulations were carried out in order to evaluate the performance of the controllers (60), (61), (74), and (75) when applied to the complete dynamics of the quadrotor transporting a suspended load given by

FIGURE 8 The oscillation  $\alpha$  angle and its projections  $\alpha_x$  and  $\alpha_y$  in the Y-Z frame and X-Z frame, respectively, and the  $\beta$  angle in the X-Y frame. [Color figure can be viewed at wileyonlinelibrary.com]

Equations (12), (13), and (14). The model parameters of the plant used in the simulations correspond to those of a real platform and are listed in Table 1. The control gains were selected according to the polynomials (76) and (76), and their values correspond to  $\lambda_0 = \omega_n^2$ ,  $\lambda_1 = 2\zeta\omega_n$  with  $\omega_n = 10$  and  $\zeta = 0.9$  for the height control and  $\gamma_0 = \omega_n^2$ ,  $\gamma_1 = 2\zeta\omega_n$  with  $\omega_n = 9$  and  $\zeta = 0.9$  for the yaw control; also,  $\rho_z = 1$  and  $\rho_y = 0.3$ . The control gains for the horizontal dynamics were selected according to polynomial (76) with  $\mathcal{K}_0 = \omega_n^6$ ,  $\mathcal{K}_1 = 6\omega_n^5\zeta$ ,  $\mathcal{K}_2 = 12\omega_n^4\zeta^2 + 3\omega_n^4$ ,  $\mathcal{K}_3 = 8\omega_n^3\zeta^3 + 12\omega_n^3\zeta$ ,  $\mathcal{K}_4 = 2\omega_n^2\zeta^2 + 3\omega_n^2$ , and  $\mathcal{K}_5 = 6\omega_n\zeta$  with  $\omega_n = 6$ ,  $\zeta = 0.9$ , and  $\rho_F = 1000$ .

The reference trajectory followed by the flats outputs  $F_x$ ,  $F_y$ ,  $z$ , and  $\psi$  is shown in Figure 5; in Figure 6, the yaw angle and the yaw reference angle are shown for the first 3 s of simulation. Also, external disturbances  $\vartheta_{F_x}(t)$ ,  $\vartheta_{F_y}(t)$ ,  $\vartheta_z(t)$ , and  $\vartheta_\psi(t)$  were introduced at  $t = 25$  s of simulation as aleatory signals, as it is shown in Figure 7.

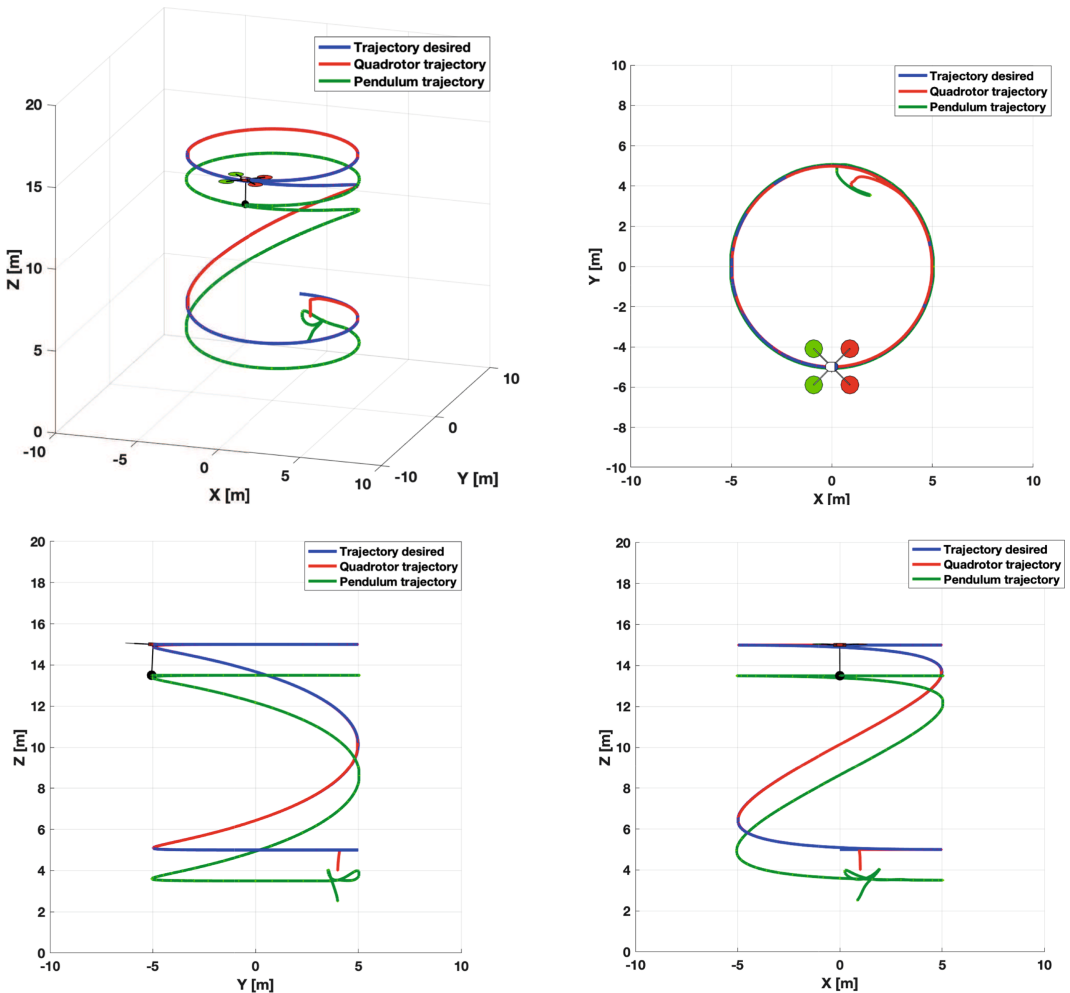


**FIGURE 12** Trajectory tracking of the quadrotor with suspended load in the three-dimensional space. [Color figure can be viewed at [wileyonlinelibrary.com](http://wileyonlinelibrary.com)]

In Figure 8, the  $\alpha$  angle and its projections in the  $X$ - $Z$  and  $Y$ - $Z$  frames are shown, as well as the  $\beta$  angle which is projected in the  $X$ - $Y$  frame. The  $\beta$  angle shows an interesting behavior (this angle only appears for the case of the spherical pendulum in three dimensions and describes the orientation of the pendulum on the frame  $X$ – $Y$  projected on the floor); under an oscillation of the pendulum, the  $\beta$  angle does not converge to zero; it only rotates around the axis  $Z_B$ . The angle that is attenuated by the control action proposed in this work is the  $\alpha$  angle.

The trajectory tracking errors  $e_{F_x}$ ,  $e_{F_y}$ ,  $e_z$ , and  $e_\psi$  are shown in Figure 9, as well as the trajectory tracking error for the yaw angle  $e_\psi$ . The attitude angles of the quadrotor are shown in Figure 10, and the control signals of the thrust force and the torques acting on the Euler angles are shown in Figure 11. Finally, in Figure 12, the behavior of the quadrotor carrying a suspended load and following the desired reference in the three-dimensional space is shown; the corresponding behavior of the quadrotor in each reference frame is also shown in that figure. A

video of an animation corresponding to the simulation can be found online (<https://www.youtube.com/watch?v=PubmTtOuENY>).

One of the main problems when considering a control based on sliding modes, when applied to a system such as the quadrotor, is the high frequency of the control signals (behavior also known in the literature as “chattering”). It is important to avoid or diminish this problem by providing continuous and smooth control signals that retain the robustness and insensitivity of the closed-control system to bounded modeled uncertainties and external disturbances. One solution is to approximate the discontinuous function  $\text{sign}(v)$  by some continuous function [48]. For instance, the function  $\text{sign}(v)$  could be replaced by

$$\frac{v}{|v| + \epsilon}, \quad (92)$$

where  $\epsilon$  is small positive scalar, for which it can be observed that

$$\lim_{\epsilon \rightarrow 0} \frac{v}{|v| + \epsilon} = \text{sign}(v). \quad (93)$$

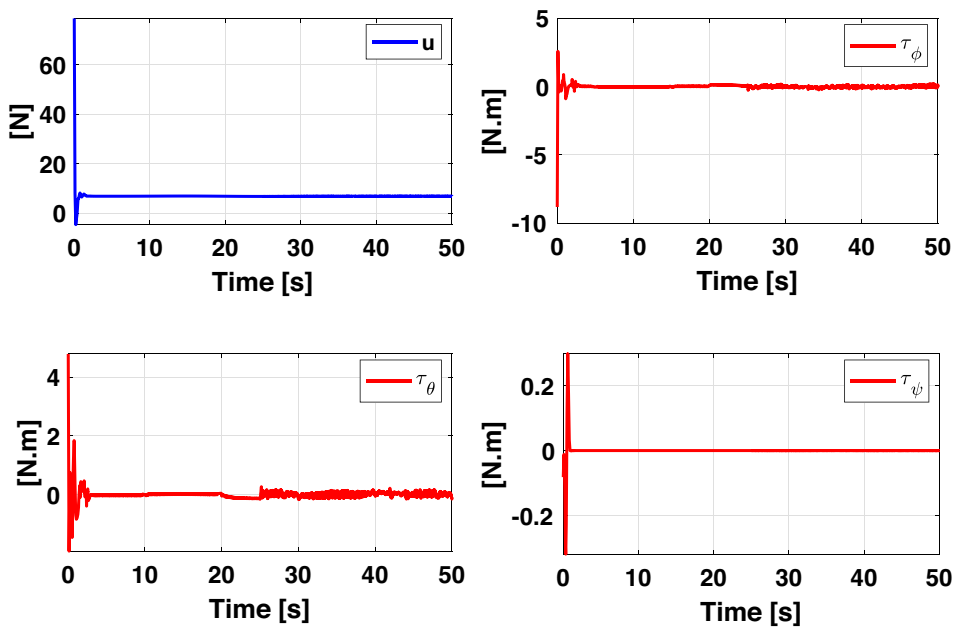


**FIGURE 13** Chattering attenuation of the control signals  $u$ ,  $\tau_\phi$ ,  $\tau_\theta$ , and  $\tau_\psi$ . [Color figure can be viewed at [wileyonlinelibrary.com](http://wileyonlinelibrary.com)]

**TABLE 2** Performance results of the controller.

| Variable   | RMS          | ISE                   |
|------------|--------------|-----------------------|
| $e_{F_x}$  | 0.0900 (m)   | 0.4883 (m)            |
| $e_{F_y}$  | 0.1240 (m)   | 0.7687 (m)            |
| $e_z$      | 0.0479 (m)   | 0.1143 (m)            |
| $e_\psi$   | 0.0584 (rad) | 0.0013 (rad)          |
| $\alpha$   | 0.11 (rad)   | 0.6051 (rad)          |
| $\alpha_x$ | 0.0699 (rad) | 0.2444 (rad)          |
| $\alpha_y$ | 0.0923 (rad) | 0.4263 (rad)          |
| $\beta$    | 10.48 (rad)  | $5.49 \times 3$ (rad) |

Abbreviations: ISE, integral square error; RMS, root mean square.

The same numerical simulation described above was carried out using (92) instead of the function  $\text{sign}(v)$ . Figure 13 shows the corresponding control signals with  $\epsilon = 1$ . In the figure, it can be observed that there is chattering attenuation, mainly in the time range where there are not external disturbances (first 25 s of simulation). When external disturbances are introduced, the control signals show small chattering and they still accomplish robust performance; that is, rejection of the external disturbances is achieved.

#### 4.1 | Comparison with other controllers

A numerical comparison of the controller proposed in this work with respect to two of the most recent published works that address the same problem, Guerrero-Sánchez et al. [19] and Urbina-Brito et al. [34], has been made. In those works, the authors show simulation results using

control techniques based on a PD approach with coupled terms and an approach based on MPC. It is important to emphasize that in Guerrero-Sánchez et al. [19], it is proposed to control the system through the thrust force using the desired Euler angles as control inputs, thus leading to consider the rotational dynamics separately. In the present work, the system is controlled through the resulting thrust force and torques as control inputs, due to the force motors, in the same way as in Urbina-Brito et al. [34]. Table 2 summarizes the performance results for the controller proposed in the present work, where RMS and ISE stand for root mean square and integral square error, respectively. The results in Table 2 can be compared with the results shown in Table 2 in Guerrero-Sánchez et al. [19] and Table 3 in Urbina-Brito et al. [34] for a better quantitative comparison.

A main difference and important contribution of the present work is the behavior obtained for the oscillation of the angles  $\alpha$  and  $\beta$ . In comparison with Figure 2b in Guerrero-Sánchez et al. [19] and Figure 2c in Urbina-Brito et al. [34], the  $\beta$  angle does not converge to zero; this is the  $\beta$  angle that rotates around the  $Z_B$  axis (see Figure 8). Therefore, the angle of interest that converges to zero, guaranteeing minimum oscillations, is the  $\alpha$  angle.

Another important point to highlight is the applicability and programming on a real-time platform. Unlike Urbina-Brito et al. [34], the present work gives a simple and easy to implement control strategy that can be programmed in a microcontroller or operating system that operates a quadrotor in real time. Experiments on a real time platform are planned to be carried out in the future.

## 5 | CONCLUSIONS

This article proposes a solution to the quadrotor system transporting a suspended load in a three-dimensional space. Unlike our previous work [45], where the problem is addressed in two dimensions, the main advantage of the control strategy proposed here is the easy implementation due to the fact that all the measurements of the system are available. The proposed dynamic model, where the oscillation dynamics of the suspended load is added to the quadrotor dynamics, has the same behavior as a spherical pendulum. One contribution in this article is the solution proposed which consists in decoupling the system dynamics, that is, the horizontal and vertical translational dynamics and the yaw dynamics. The horizontal translational dynamics are addressed in two frames, namely, in a  $X$ - $Z$  frame and  $Y$ - $Z$  frame. This simplification allows to approach the problem using an approximate linearization of the system model together with the flatness concept, since the approximate linearized model is found to be controllable around an arbitrary equilibrium point. With the use of the flatness property of the approximately linearized system, it was found that this linear system can be decoupled into the horizontal and vertical dynamics; thus, each control input only has an effect on the vertical and horizontal motions. This fact lead to address the vertical dynamics by means of a robust control law based on the nonlinear model to guarantee that all the variables associated with the vertical movement are attracted to zero including the yaw dynamics. On the other hand, the horizontal dynamics is addressed using the linear flat output in the axes  $X$  and  $Y$ . Due to the robustness and high insensitivity to parameter variations and internal and external disturbances of the system, the sliding mode control scheme was proposed for the four dynamics (in the  $X$ - $Z$  and  $Y$ - $Z$  frames, the vertical dynamics or height control, and the yaw dynamics). Another important contribution is the solution provided by the dynamics of motion of the suspended load in three dimensions; these dynamics correspond to a spherical pendulum that moves in the space by means of a quadrotor. In this sense, it is important to emphasize that when carrying out numerical simulations of the resultant closed-loop system, the  $\beta$  angle, unlike many published works, does not converge to zero. That is, it is physically impossible that under a circular oscillation of the suspended load in the  $X$ - $Y$  frame, the  $\beta$  angle do not converge to zero by means of the control action; this angle increases over time. Only the  $\alpha$  angle converges to zero, guaranteeing the attenuation of the oscillations of the suspended load.

From the simulations results, it can be observed that trajectory tracking of the quadrotor and the load is performed with small and bounded tracking errors while keeping the

swinging of the suspended load within small bounds. The control signals were kept bounded although the chattering effect has a high frequency; however, it has been shown that it is possible to attenuate the effect of chattering or high frequency in the control signals, using an approximation of the discontinuous function. In order to evaluate the performance of the control strategy proposed here, experiments on a real time platform are planned to be carried out in the future.

## AUTHOR CONTRIBUTIONS

The author contribution of each author has been equal in the methodology, research, writing-review, and editing of the article.

## ACKNOWLEDGMENTS

This work was supported by CONAHCYT Mexico and CINVESTAV.

## CONFLICT OF INTEREST STATEMENT

The authors declare that there is no competing financial interest or personal relationship that could have appeared to influence the work reported in this paper.

## ORCID

*Adrian Humberto Martinez-Vasquez*  <https://orcid.org/0000-0001-5837-787X>

*Rafael Castro-Linares*  <https://orcid.org/0000-0002-9227-4505>

## REFERENCES

1. N. Boonyathanngig, S. Gongmanee, P. Kayunyeam, P. Wutticho, and S. Prongnuch, *Design and implementation of mini-UAV for indoor surveillance*, 2021 9th International Electrical Engineering Congress (IEECON), 2021, pp. 305–308.
2. J.-H. Park, S.-C. Choi, I.-Y. Ahn, and J. Kim, *Multiple UAVs-based surveillance and reconnaissance system utilizing IoT platform*, 2019 International Conference on Electronics, Information, and Communication (ICEIC), 2019, pp. 1–3.
3. D. N. Cardoso, S. Esteban, and G. V. Raffo, *A new robust adaptive mixing control for trajectory tracking with improved forward flight of a tilt-rotor UAV*, ISA Trans. **110** (2021), 86–104.
4. D. Invernizzi and M. Lovera, *Trajectory tracking control of thrust-vectoring UAVs*, Automatica **95** (2018), 180–186.
5. K. Xia, W. Chung, and H. Son, *Dynamics estimator based robust fault-tolerant control for VTOL UAVs trajectory tracking*, Mech. Syst. Sig. Process. **162** (2022), 108062.
6. B. J. Perry and Y. Guo, *A portable three-component displacement measurement technique using an unmanned aerial vehicle (UAV) and computervision: a proof of concept*, Measurement **176** (2021), 109222.
7. P. Sun, B. Zhu, Z. Zuo, and M. V. Basin, *Vision-based finite-time uncooperative target tracking for UAV subject to actuator saturation*, Automatica **130** (2021), 109708.

8. A. R. Vetrella, G. Fasano, and D. Accardo, *Attitude estimation for cooperating UAVs based on tight integration of GNSS and vision measurements*, *Aerosp. Sci. Technol.* **84** (2019), 966–979.
9. Z. A. Ali and X. Li, *Controlling of an under-actuated quadrotor UAV equipped with a manipulator*, *IEEE Access* **8** (2020), 34664–34674.
10. J. Fishman and L. Carbone, *Control and trajectory optimization for soft aerial manipulation*, 2021 IEEE Aerospace Conference (50100), 2021, pp. 1–17.
11. N. Zhao, Y. Luo, H. Deng, Y. Shen, and H. Xu, *The deformable quad-rotor enabled and wasp-pedal-carrying inspired aerial gripper*, 2018 IEEE/RSJ International Conference on Intelligent Robots and Systems (IROS), 2018, pp. 1–9.
12. J. Ghommam, A. Chemori, and F. Mnif, Finite-time stabilization of underactuated mechanical systems in the presence of uncertainties: application to the cart-pole system, *The inverted pendulum in control theory and robotics: from theory to new innovations*, Vol. **Chapter 8**, 2017, pp. 165–187.
13. T. Ishida, T. Oshiro, and T. Nagado, *Sliding mode control of an inverted pendulum: comparison on robustness between a sliding mode control and an optimal regulator*, *IFAC Proc. Vol.* **23** (1990), no. 8, Part 4, 317–322. 11th IFAC World Congress on Automatic Control, Tallinn, 1990 - Volume 4, Tallinn, Finland.
14. R. Lozano and I. Fantoni, Passivity based control of the inverted pendulum, *Perspectives in control: theory and applications*, D. Normand-Cyrot, (ed.), Springer London, London, 1998, pp. 83–95.
15. B. Barikbin and A. Fakharian, *Trajectory tracking for quadrotor UAV transporting cable-suspended payload in wind presence*, *Trans. Inst. Meas. Control* **41** (2019), no. 5, 1243–1255.
16. M. E. Guerrero, D. A. Mercado, R. Lozano, and C. D. García, *IDA-PBC methodology for a quadrotor UAV transporting a cable-suspended payload*, 2015 International Conference on Unmanned Aircraft Systems (ICUAS), 2015, pp. 470–476.
17. M. E. Guerrero, D. A. Mercado, R. Lozano, and C. D. García, *Passivity based control for a quadrotor UAV transporting a cable-suspended payload with minimum swing*, 2015 54th IEEE Conference on Decision and Control (CDC), 2015, pp. 6718–6723.
18. M. E. Guerrero-Sánchez, D. A. Mercado-Ravell, R. Lozano, and C. D. García-Beltrán, *Swing-attenuation for a quadrotor transporting a cable-suspended payload*, *ISA Trans.* **68** (2017), 433–449.
19. M. E. Guerrero-Sánchez, R. Lozano, P. Castillo, O. Hernández-González, C. D. García-Beltrán, and G. Valencia-Palomo, *Non-linear control strategies for a UAV carrying a load with swing attenuation*, *Appl. Math. Model.* **91** (2021), 709–722.
20. A. Mosco-Luciano, R. Castro-Linares, and H. Rodríguez-Cortés, *Trajectory tracking control for a quadrotor with a slung load*, 2020 International Conference on Unmanned Aircraft Systems (ICUAS), 2020, pp. 322–328.
21. X. Liang, Y. Fang, N. Sun, H. Lin, and X. Zhao, *Adaptive nonlinear hierarchical control for a rotorcraft transporting a cable-suspended payload*, *IEEE Trans. Syst., Man, Cybern.: Syst.* **51** (2021), no. 7, 4171–4182.
22. O. Bingöl and H. M. Güzey, *Sliding mode control for a quadrotor UAV transporting a cable-suspended payload*, 2020, pp. 289–303.
23. L. Sun, K. Wang, A. H. A. Mishamandani, G. Zhao, H. Huang, X. Zhao, and B. Zhang, *A novel tension-based controller design for the quadrotor load system*, *Control Eng. Pract.* **112** (2021), 104818. <https://www.sciencedirect.com/science/article/pii/S0967066121000952>
24. J. E. Sierra-García and M. Santos, *Intelligent control of an UAV with a cable-suspended load using a neural network estimator*, *Expert Syst. Appl.* **183** (2021), 115380. <https://www.sciencedirect.com/science/article/pii/S095741742100806X>
25. X. Liang and Y. Hu, *Tracking control and differential flatness of quadrotor with cable-suspended load*, 2019 IEEE 3rd Information Technology, Networking, Electronic and Automation Control Conference (ITNEC), 2019, pp. 88–92.
26. P. Kotaru, G. Wu, and K. Sreenath, *Differential-flatness and control of quadrotor(s) with a payload suspended through flexible cable(s)*, 2018 Indian Control Conference (ICC), 2018, pp. 352–357.
27. Y. Ping, J. Qi, and C. Wu, *Quadrotor transporting cable suspended load using ADRC*, 2019 Chinese Control Conference (CCC), 2019, pp. 8008–8013.
28. Z. Wang, J. Qi, C. Wu, M. Wang, Y. Ping, and J. Xin, *Control of quadrotor slung load system based on double ADRC*, 2020 39th Chinese Control Conference (CCC), 2020, pp. 6810–6815.
29. G. Minhuan, D. Gu, W. Zha, X. Zhu, and Y. Su, *Controlling a quadrotor carrying a cable-suspended load to pass through a window*, *J. Intell. Robot. Syst.* **98** (2020), 387–401.
30. T. Gaetano, E. D'Amato, M. Ariola, P. S. Rossi, and T. A. Johansen, *Model predictive control for a multi-body slung-load system*, *Robot. Autonom. Syst.* **92** (2017), 1–11.
31. C. Y. Son, T. Kim, S. Kim, and H. J. Kim, *Model predictive control of a multi-rotor with a slung load for avoiding obstacles*, 2017 14th International Conference on Ubiquitous Robots and Ambient Intelligence (URAI), 2017, pp. 232–237.
32. J. B. Ubbink and J. A. A. Engelbrecht, *Sequence-constrained trajectory planning and execution for a quadrotor UAV with suspended payload*, *IFAC-PapersOnLine* **53** (2020), no. 2, 9405–9411. 21st IFAC World Congress.
33. H. Danial and H. Hamidreza, *Trajectory planning of quadrotor UAV with maximum payload and minimum oscillation of suspended load using optimal control*, *J. Intell. Robot. Syst.* **100** (2020), 1369–1381, DOI 10.1007/s10846-020-01166-4.
34. N. Urbina-Brito, M.-E. Guerrero-Sánchez, G. Valencia-Palomo, O. Hernández-González, F.-R. Lopez-Estrada, and J. A. Hoyo-Montano, *A predictive control strategy for aerial payload transportation with an unmanned aerial vehicle*, *Mathematics* **9** (2021), no. 15. <https://www.mdpi.com/2227-7390/9/15/1822>
35. M. E. Guerrero-Sánchez, O. Hernández-González, G. Valencia-Palomo, D. A. Mercado-Ravell, F. R. Lopez-Estrada, and J. A. Hoyo-Montano, *Robust IDA-PBC for under-actuated systems with inertia matrix dependent of the unactuated coordinates: application to a UAV carrying a load*, *Nonlinear Dyn.* **105** (2021), 3225–3238, DOI 10.1007/s11071-021-06776-7.
36. A. R. Godbole and K. Subbarao, *Nonlinear control of unmanned aerial vehicles with cable suspended payloads*, *Aerosp. Sci. Technol.* **93** (2019), 105299. <https://www.sciencedirect.com/science/article/pii/S1270963818325185>
37. G. E. M. Abro, S. A. Bin Mohd Zulkifli, and V. S. Asirvadam, *Dual-loop single dimension fuzzy-based sliding mode control design for robust tracking of an underactuated quadrotor craft*, *Asian J. Control* **25**, no. 1, 144–169, DOI 10.1002/asjc.2753.
38. H. Sira Ramírez, M. A. Aguilar-Ordua, and B. C. Gómez-Len, *Sliding mode control of switched systems: a geometric algebra approach*, *Asian J. Control* **25** (2023), no. 1, 15–25, DOI 10.1002/asjc.2781.

39. X. Hu, C. Guo, C. Hu, and B. He, *Sliding mode learning control for t-s fuzzy system and an application to hypersonic flight vehicle*, Asian J. Control **25** (2023), no. 1, 407–417, DOI 10.1002/asjc.2822.
40. H. Sira-Ramírez and S. K. Agrawal, *Differentially flat systems*, 2004.
41. P. Castillo and A. Dzul, Aerodynamic configurations and dynamic models, *Unmanned aerial vehicles*, John Wiley & Sons, Ltd, 2013, pp. 1–20.
42. S. Bouabdallah, *Design and control of quadrotors with application to autonomous flying*, 2007.
43. Y. Zou, *Nonlinear hierarchical control for quad-rotors with rotation matrix*, Int. J. Control **90** (2017), no. 7, 1308–1318, DOI 10.1080/00207179.2016.1205756.
44. M. Fließ, J. Lvine, P. Martin, and P. Rouchon, *Flatness and defect of non-linear systems: introductory theory and examples*, Int. J. Control **61** (1995), 13–27.
45. A. H. Martinez-Vasquez, R. Castro-Linares, and A. E. Rodriguez-Mata, *Sliding mode control of a quadrotor with suspended payload: a differential flatness approach*, 2020 17th International Conference on Electrical Engineering, Computing Science and Automatic Control (CCE), 2020, pp. 1–6.
46. S. J. Utkin Vadim, *Sliding mode control in electro-mechanical systems*, 2009.
47. H. K. Khalil, *Nonlinear systems*; 3rd ed, Prentice-Hall, Upper Saddle River, NJ, 2002.
48. Y. Shtessel, C. Edwards, L. Fridman, and A. Levant, *Sliding mode control and observation*, 2014. 291–320.

## AUTHOR BIOGRAPHIES



**Adrian Humberto Martinez-Vasquez** received his bachelor's degree in Mechatronic Engineering from the Technological University of the Mixteca, Oaxaca, Mexico, from 2007 to 2012 and his M.S. degree in autonomous air and submarine navigation systems from LAFMIA UMI CNRS 3175 - CINVESTAV, Mexico, and he is a Ph.D. candidate in

Electrical Engineering in the Department of Electrical Engineering at CINVESTAV, Mexico.



**Rafael Castro-Linares** received his B.S. degree in Communications and Electronics Engineering from the National Polytechnic Institute, Mexico City, Mexico, his M.S. degree in Electrical Engineering from CINVESTAV, Mexico City, Mexico, and his Ph.D. degree in Electrical Engineering, from CINVESTAV, Mexico City, Mexico, in 1981, 1982, and 1987, respectively. He is currently a professor in the Department of Electrical Engineering of CINVESTAV, Mexico City. He has held visiting positions at Laboratoire d'Automatique de Grenoble, INPG, Grenoble, France, Dipartimento d' Informatica e Sistemistica, University of Rome "La Sapienza", Rome, Italy, Institut de Recherche en Communications et Cybernétique de Nantes, Nantes, France, Faculty of Applied Mathematics, University of Twente, Enschede, The Netherlands, and the Department of Electrical Engineering, Universidad de Chile, Santiago, Chile. Prof. Castro-Linares is also a Senior Member of the IEEE (Institute of Electrical and Electronics Engineers). His research interests lie in the theory and practice of nonlinear control.

**How to cite this article:** A. H. Martinez-Vasquez and R. Castro-Linares, *Flatness-based sliding mode control for stabilizing a spherical pendulum on a quadrotor*, Asian J. Control. (2024), 1–17, DOI 10.1002/asjc.3308.